Available online at www.sciencedirect.com
ScienceDirect
Catalysis Today 120 (2007) 107–120
CATALYSIS TODAY
www.elsevier.com/locate/cattod

Water Gas Shift Reaction in a glass microreactor

S. Mukherjee [a], M.K. Hatalis [b], M.V. Kothare [a,*]

[a] Department of Chemical Engineering, Lehigh University, 111 Research Drive, Bethlehem, PA 18015, USA
[b] Department of Electrical and Computer Engineering, Lehigh University, 16A Fairchild Laboratory, Bethlehem, PA 18015, USA

Available online 17 August 2006

Abstract

A micro scale glass reactor was designed, fabricated and characterized with Water Gas Shift Reaction (WGSR). The fabrication procedure was quick, uncomplicated, template-free and inexpensive and did not require any special clean room facility, making it ideal for first generation prototyping. The fabricated unit was able to withstand pressure and temperature of 1.65 MPa and 260 °C respectively. An important reaction in micro scale fuel processing, namely WGSR, was carried out in this microreactor using a packed bed of 50–75 μm commercial catalyst particles at 185–250 °C. The design sizing was based on a CO flow of 0.06 mol/h. Experimental results were used to develop a kinetic model of the reaction.

Keywords: Water Gas Shift Reaction; Glass microreactor; Catalyst activation

1. Introduction

Micro scale chemical units have generated a great deal of interest in the last decade. The principal benefits of miniaturization are improved heat and mass transfer [1–3], increased space–time yield [4], increased reaction selectivity control [5] and the ability to handle dangerous chemicals more safely. These advantages have been exploited for a number of novel applications. Several attempts [6–8] have been made to number up the micro devices for large scale production. Others have proposed research applications, such as catalyst screening [9]. Still others have proposed a compact stand-alone chemical system or plant-on-a-chip. One such application of considerable interest in recent years is a micro fuel processor plant-on-a-chip to generate hydrogen for micro fuel cells that can power portable electronic devices.

Portable digital devices are getting smaller, more versatile and energy intensive, but the limitation of current battery technology hinders further miniaturization and intensification. Micro fuel cells are considered as candidate portable power sources to replace bulky lithium ion batteries [10,11]. Fuel cells work most efficiently on hydrogen. However, as a stored energy medium, hydrogen is not ideal due to its extremely low energy density and hazards of storage. Methanol, on the other hand, is excellent because of its higher energy density and can be steam reformed to produce hydrogen *in situ* in micro fuel processors for use in micro fuel cells.

A number of micro scale steam reformer designs have been proposed and fabricated (see Refs. [12–15]). In a steam reformer, methanol and steam react to produce hydrogen and carbon dioxide, and also significant amounts of carbon monoxide as byproduct. Carbon monoxide (CO) poisons the catalyst in fuel cells and therefore, the reformate stream needs to be further treated to remove CO. While high temperature fuel cell membranes that are tolerant to CO are currently being investigated, in general, purifying the hydrogen stream using a micro-membrane and removing CO using Water Gas Shift Reaction (WGSR) remain important design options in micro-reformers (see Karnik et al. [16]).

WGSR refers to the reaction of CO and steam to produce hydrogen and carbon dioxide. This is an important reaction used widely in the traditional chemical industry. More recently it has found application in purifying hydrogen for small scale fuel cells. Various mechanisms, reaction paths and reaction rates have been reported in literature [17–19]. For this system, however, the specific expressions fit specific experimental data and experimental set-ups, but vary widely with reactor size [20,21] and reaction conditions [22]. For example, rate expressions for large WGS reactors operating at high temperature and pressure could be different from those estimated in a microreactor.

Several attempts at fabricating WGS microreactor have been made in the past. Goerke et al. [23] have coated metal micro

* Corresponding author. Tel.: +1 610 758 6654; fax: +1 610 758 5057.
E-mail address: mayuresh.kothare@lehigh.edu (M.V. Kothare).

0920-5861/$ – see front matter
doi:10.1016/j.cattod.2006.07.007

Nomenclature

A	pre-exponential constant
A_c	cross-sectional area (m^2)
C	concentration of reactants and products (mol/l)
C_B	concentration of reactant ''B'' at any point in the reactor
D_{ab}	diffusivity constant (m^2/s)
D_P	diameter of particle
E	activation energy of reaction (J/mol)
K	reaction constant for WGSR
K'	constant from pressure drop correlation ($s\ m^{-4}$)
K''	permeability constant from Darcy's law (m^2)
K_{eq}	equilibrium constant for WGSR
K_{exp}	modified reaction constant
l	a point along the length of the reactor (m)
L	length of reactor (m)
M	molar ratio of water and carbon monoxide
n_B	molar flow rate of reactant/product B (mol/s)
n^0_{CO}	molar flow rate of CO at inlet (mol/s)
$n^0_{H_2O}$	molar flow rate of steam at inlet (mol/s)
P	pressure at any point (Pascal (Pa) or pound-per-square-inch (psi))
p_{CO}	partial pressure of carbon monoxide (bar)
p_{CO_2}	partial pressure of carbon dioxide (bar)
p_{H_2}	partial pressure of hydrogen (bar)
p_{H_2O}	partial pressure of steam (bar)
P_i	inlet pressure (Pa)
P_o	outlet pressure (Pa)
P_0	pressure at NTP, or 1 atm
R	universal gas constant (J/mol/K)
T	temperature (Kelvin (K))
T_0	temperature at NTP, or 298 K
$\mathbf{u}$	velocity vector (m/s)
v_g	gas velocity (m/s)
V	volumetric flow rate (l/min)
V_0	volumetric flow rate at NTP
W	weight of catalyst (g)
X	fractional conversion of CO with respect to initial CO concentration
X_L	fractional conversion of CO at outlet
X_1, X_2	roots of quadratic Eq. (7)

Greek letters

ϕ	porosity
μ	viscosity (Pa s)

channel walls with WGSR catalyst. Similarly, Bravo et al. [24] have coated glass tubes with WGSR catalyst. This method reduces effective pressure drop, but the required residence time in the reactor increases.

The principal materials used for fabricating micro scale chemical units are silicon, metal, glass, various polymers and ceramics. Silicon has generated a great deal of interest due to the small feature size that can be achieved and the wealth of knowledge that has been gathered from the micro electro-mechanical systems (MEMS) fabrication research. One of the significant advances in micro scale chemical systems is the advent of micro scale sensors and actuators such as micro-pumps, piezoelectric actuators, RTD sensors and micro valves which are unique to silicon based fabrication.

The numerous advantages of using silicon are negated by the high cost of material and fabrication in clean rooms. This fact becomes significant as the size of the unit becomes larger. Compact hand held chemical devices will always be significantly larger than silicon based electronic microchips due to physical limitations. This is because, smaller fluidic channels lead to larger pressure drop and furthermore reaction conversion is constrained by reactor volume requirements. Thus, commercially viable micro chemical units may not necessarily use silicon as the principal material of construction.

Glass is a well-suited material for prototyping micro scale hand held chemical devices. Various methods of machining glass cheaply outside the clean room exist. Glass is transparent and allows easy visual inspection and spectroscopic reaction studies. Glass is also chemically inert to most reagents with the exception of hydrofluoric acid, hot phosphoric acid and hot alkali. And finally, as compared to metals, polymers or ceramics, glass has the distinct advantage of being compatible with silicon and can be readily bonded to silicon wafers and devices, thereby providing integrated functionality.

Glass based mixers, reactors and heat exchangers have been produced by LTF GmbH[1] and Micronit.[2] Brivio et al. [25] used similar reactors to test surface effects in acid esterification. Fletcher et al. [5] used a glass reactor to control flow electrokinetically and to carry out reaction. Glass based fabrication is usually done using sand blasting or hydrofluoric acid (HF) based wet etching. Both these methods produce slanted channel walls. Deep Reactive Ion Etching (DRIE) has been used to etch glass, but etch rates are slow [26]. Photo-etchable glass, Foturan, developed by Schott[3] can be used to make feature sizes as small as 25 μm. Dietrich et al. [27] and Cho et al. [28] have discussed various applications of Foturan.

Though the eventual material of choice for fabricating disparate units remains unclear, it is evident that a study of glass as a material for low cost fabrication and prototyping of microchemical units is well justified.

The goal of this paper is to: (1) explore the use of glass as a material for fabrication of low cost, first generation micro-reactor prototypes, (2) fabricate and characterize the glass microreactor and microfluidic interconnector using template-free, cheaper fabrication tools, and (3) characterize the rate expression for Water Gas Shift Reaction in the fabricated glass microreactor to facilitate future microreactor designs.

This paper is organized as follows: in Section 2, the Water Gas Shift Reaction is discussed. In Section 3, design criteria and fabrication steps of the microreactor are presented. A

[1] http://www.ltf-gmbh.de/en/.
[2] http://www.micronit.com/.
[3] http://www.us.schott.com/english/index.html.

micro-vaporizer and a micro-mixer are also proposed. For this work, channels and holes in glass are machined using a vertical drilling machine. Characterization results of the fabricated unit are explained in Section 4. Reaction set-up and results are presented in Section 5.

2. Water Gas Shift Reaction

Water Gas Shift Reaction refers to the chemical reaction between carbon monoxide (CO) and water (H_2O) to produce hydrogen (H_2) and carbon dioxide (CO_2). This reaction is usually carried out on a metal oxide catalyst. Commercially, the two common catalysts used are iron oxide based and copper based. For our study, the low temperature $CuO/ZnO/Al_2O_3$ catalyst from ICI-Synetix (Katalco 83-3K) was used. The chemical reaction is stated as:

$$CO + H_2O \rightleftharpoons H_2 + CO_2 \quad \Delta H = -41.17\,\text{kJ/mol}. \tag{1}$$

The reaction is exothermic as indicated by the negative heat load (ΔH). The reaction is reversible with the equilibrium constant, K_{eq}, given by Moe [29]:

$$K_{eq} = \exp\left(\frac{4577.8}{T} - 4.33\right), \tag{2}$$

where the temperature, T, is in Kelvin. The reaction rate equation assumed for this work can be stated as

$$r_{CO} = -K\left(C_{CO}C_{H_2O} - \frac{C_{H_2}C_{CO_2}}{K_{eq}}\right). \tag{3}$$

Based on plug flow idealization, the rate equation above was converted into the differential model

$$n^0_{CO}\frac{dX}{dl} = \frac{W}{L}K\left(C_{CO}C_{H_2O} - \frac{C_{H_2}C_{CO_2}}{K_{eq}}\right), \tag{4}$$

where l is the length co-ordinate along the plug flow microreactor, and $l = 0$ and $l = L$ are the microreactor inlet and outlet respectively. Subscripts denote the chemical species. The molar flow rate, molar concentration, weight of catalyst and reaction rate constant are given by n, C, W and K respectively. X is the fractional conversion of CO with respect to initial CO concentration and n^0_{CO} is the inlet molar flow rate of CO.

The objective of this study is to find the reaction rate constant, K which varies with temperature, T, as,

$$K = A\exp\left(-\frac{E}{RT}\right). \tag{5}$$

Here R is the universal gas constant, and A and E are the pre-exponential factor and activation energy, respectively, that need to be evaluated.

By analytically integrating Eq. (4) and incorporating the pressure variation along the length of the reactor (see Eq. (14)), we get (see derivation in Appendix A),

$$A\exp\left(-\frac{E}{RT}\right) = \frac{2(1+M)^2(RT)^2 n^0_{CO}}{W(P_i^2 + P_o^2)\sqrt{(1-M)^2 + (4M/K_{eq})}}\ln\left(\frac{(X_2 - X_L)X_1}{(X_1 - X_L)X_2}\right). \tag{6}$$

Here X_L is the CO conversion at the exit and, X_1 and X_2 are the roots of the quadratic equation,

$$(1-X)(M-X) - \frac{X^2}{K_{eq}} = 0. \tag{7}$$

Reduced particle size leads to significant pressure drop that should be accounted for in the analysis of the rate constant. This formulation (Eq. (6)) therefore specifically incorporates the effect of pressure variation along the length of the reactor.

3. Design and fabrication

The goal of miniaturization is to perform multiple unit operations in a compact (micro) unit. In our proposed WGS microreactor four operations were carried out—heating, mixing, vaporization and reaction. The size of the unit was based on a flow rate of 0.06 mol/h of CO. The geometry is planar and consists of three glass wafers. The unit is heated on a hot plate and is fabricated to withstand moderately high temperature. The temperature ratings of all the components are given in Table 1. The planar geometry significantly reduced temperature gradients in our application. In addition, applying Mears's criterion to our microreactor configuration under the operating conditions described by Mears [21], we anticipate that reaction rate deviation from isothermal conditions will be small.

There are two inlet ports for the inflow of carbon monoxide (gas) and water (liquid) and an outlet port (see Fig. 1). Evaporation of water to steam requires special care and has been described in depth in Section 3.6. The fluids enter rectangular cross-section channels of dimension 2000 μm × 100 μm. In these channels, carbon monoxide and steam are heated. The length of the channels is long enough to heat the reactants to reactor temperature before reaching the packed bed catalyst. The two gas streams intersect at a micro-mixer described in more detail in Section 3.5. Two narrow rectangular glass wool sections are placed between the narrow channelled heating section and the broader reactor to help fluid distribution. Furthermore glass wool packing helps retain the catalyst.

Table 1
Temperature rating of materials as reported by their manufacturers

Fabrication material	Maximum operating temperature (°C)
Schott borosilicate glass	450
Teflon PTFE tube	260
Glass wool	340
High temperature epoxy	315

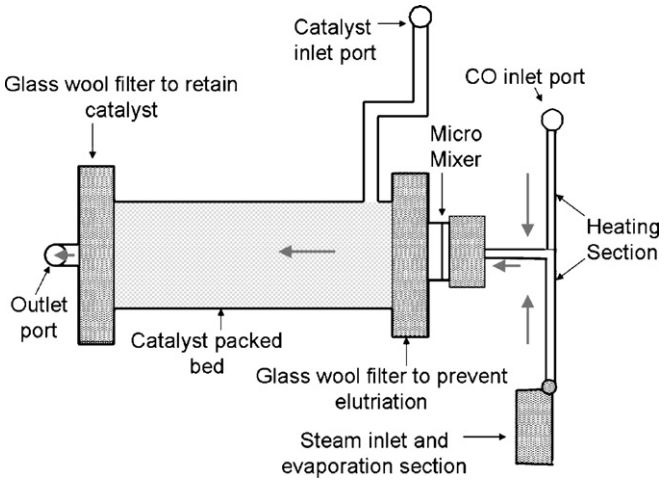

Fig. 1. Planar diagram of WGS microreactor.

The dimensions of the rectangular microreactor, i.e. length (L) and width (W) were determined by the reaction conversion requirement and pressure drop considerations. For design purposes, an approximate reactor volume was calculated by using the reaction rate proposed by Keiski et al. [30]. Pressure drop measurements in a test reactor with the proposed catalyst provided the pressure drop correlation. The height (H) was chosen to be 400 μm. Smaller height could lead to catalyst clogging while larger height could lead to non-isothermal heat transfer (see Ref. [31]). Based on these assumptions, the required length of 4 cm and width of 1.7 cm was found to be adequate. The advantages of having a broader reactor as opposed to a longer one have been discussed in Ajmera et al. [9]. The microreactor with the above dimensions was packed with commercial catalyst from Synetix.

3.1. Experimental procedure

Fig. 2 shows a schematic of the experimental set-up. Water was pumped into the reactor using a syringe pump while CO was fed in through a flow controller (from Aalborg[4]). A pressure sensor placed between the flow controller and the reactor measured the upstream pressure. The effluent from the reactor was passed through a water collector to condense the unreacted steam. An inert gas (argon) of known flow rate was mixed with the rest of the exhaust gas before feeding to a mass spectrometer (Stanford Research System's QMS-200 gas analyzer[5]). The gas analyzer provides real time analysis of the composition of the effluent gas from the microreactor. The temperature of the microreactor was maintained at the desired level by placing it on a hot plate. There is a difference between the top and bottom of the glass microreactor of approximately 13 °C. The reactor was assumed to be 5 °C below the hot plate temperature.

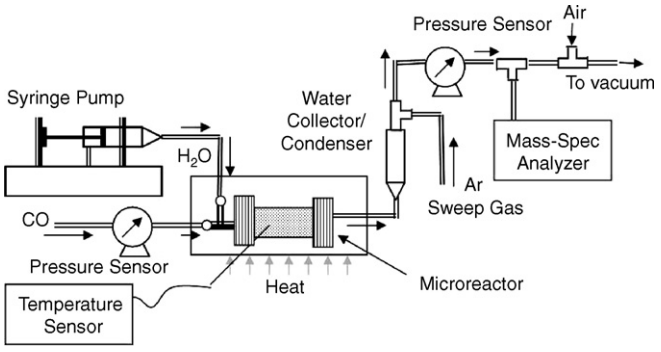

Fig. 2. Flow sheet of WGS reaction.

3.2. Fabrication

The unit consists of three glass wafers 1.75 mm thick from Swift Glass.[6] The standard technique of fabricating micro-chemical systems was followed.

This consists of machining an open channel in one wafer and then capping the channel with another wafer (see Fig. 4). On two glass wafers (Wafers A and B in Fig. 3), open channels were machined with a spinning diamond drill bit (Bridgeport Vertical Drilling Machine with a diamond drill bit, spinning at 3000 rpm and continuously flooded with coolant) that was rastered over the surface. Sufficiently accurate depth control was achieved. The side walls were verified to be perpendicular under optical microscope. Fig. 5 shows the fabricated unit. A schematic of the fabrication steps is given in Fig. 4. For this design the smallest drill bit of 500 μm radius was used. However, drill bits as small as 50 μm are available commercially and can be used to develop smaller feature sizes.

In the third glass wafer (Wafer C in Fig. 3), 870 μm radius holes were drilled for the two inlet, one outlet and one catalyst filling ports. The port holes were specially drilled to allow eventual integration with a macro-micro interconnector. This is further described in the next section. In each glass wafer, two alignment holes were drilled, that were 500 μm in radii. Each hole was formed by first drilling half way through the wafer and then drilling from the other side. This technique prevented chipping.

Glass wool was placed in the filter area, mixer area and evaporation area (see Figs. 4c and 5) with its threads oriented perpendicular to the fluid flow. The wafers were then bonded together using Duralco 4460 epoxy,[7] which can withstand temperatures up to 315 °C (600 °F). A thin layer of the epoxy was spread over the wafer surface. The three wafers were held above each other and two "guide" wires were passed through the alignment holes so as to align the wafers correctly. The wafers were slid along the guide wires and then pressed against each other. Trapped air bubbles were removed by finger pressing the wafers. The guide wires were then removed. The epoxy was cured on a hot plate, successively at 120 °C for 4 h, at 175 °C for 2 h and at 220 °C for 12 h.

[4] http://www.aalborg.com/.
[5] http://www.thinksrs.com/products/QMS.htm.
[6] http://www.swiftglass.com/.
[7] http://www.cotronics.com/.

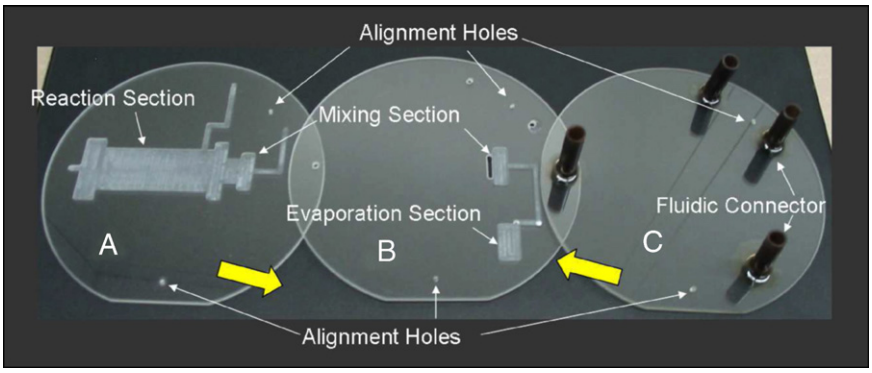

Fig. 3. Machined glass wafers used in microreactor assembly. Glass Wafers A–C are aligned using alignment holes and bonded using epoxy. In Wafer C, PTFE tubes for fluidic connector have been bonded.

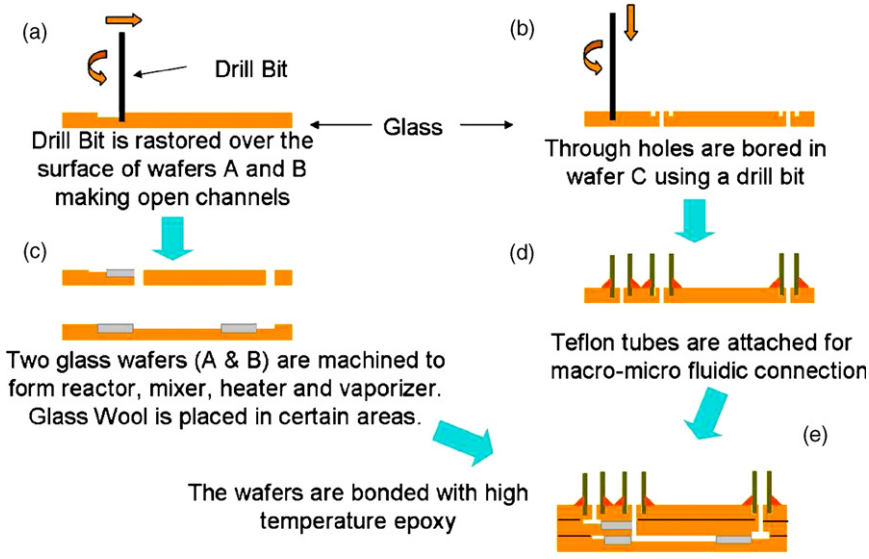

Fig. 4. Fabrication steps of the reactor.

The heating section is 2 mm in width and it opens up to a significantly broader reactor section. It is important that the flow velocity of the gas entering the reactor section is uniform. Non-uniform flow would lead to reduced reaction. Simulations have been carried out to verify this and the results are reported in Section 3.4. Furthermore, the pressure drop in the packed bed has been characterized in Section 4.3.

3.3. Macro-micro fluidic connector

For this unit, an improved connector was designed for the inlet, outlet and catalyst insertion ports. In the past macro-micro fluidic connections have been made by bonding tubes into the through hole. Various methods have evolved that typically involve forming a temporary seal before epoxy is used to make the connection permanent. Tsai and Lin [32] used a Mylar sheet for this purpose. Andersson et al. [33] melted the tubes on the silicon substrate using a roughened surface. Pattekar and Kothare [34] melted the Teflon tube in the glass hole to form an artificial O-ring. However, one limitation of their method is that if the temporary seal is not done properly, the epoxy could permanently clog the channel.

The connector proposed here is simple, economical, robust and able to withstand high temperature and pressure (see Fig. 6). Moreover, it significantly reduces the possibility of clogging the channel with epoxy, thereby overcoming a key limitation of existing fluidic connections. In Wafer C of Fig. 3, 875 μm radii through holes were bored for the ports. Around the through hole, a doughnut shaped groove, 500 μm in depth was machined using a core drill bit. The core drill bit is shaped like a hollow cylinder. The inner radius of the doughnut shaped groove is 3/32 in. (2.38 mm) and the outer radius is 9/64 in. (3.57 mm). Teflon (polytetrafluoroethylene—PTFE) tube of inner radius 3/32 in. (2.38 mm), outer radius 1/8 in. (3.175 mm) and a wall thickness of 1/32 in. was cut to a length of 2 cm. The tube was chosen such that it would sit snugly on the doughnut groove. The Teflon tube was made bondable by immersing in a fluoro polymer etchant, from FluoroEtch.[8] The immersion was for 60 s in the FluoroEtch maintained at 60 °C. Subsequently the tube was washed in acetone and water at 65 °C. This process

[8] http://www.actontech.com/fluor1.htm.

leaves the bulk of the polymer unaffected but renders the surface bondable with conventional adhesives.

One end of the Teflon tube was dipped in epoxy, Duralco 4460, and placed on the doughnut groove. The epoxy flows in the groove, but not into the through hole. The epoxy is solidified by curing at 120 °C for 2 h forming a leak-proof, temporary bond. Once the epoxy solidifies, more epoxy was poured on the outer sides of the Teflon tube and cured forming a strong bond, without leaks.

The Teflon tube was then attached to a barb-to-luer connector. A 5/32 in. polypropylene barb-to-male luer connector was procured from Harvard Apparatus.[9] The barb-side was pushed into the Teflon tube forming a strong bond. To further strengthen the connection, Duralco 4460 epoxy was used to bond the polypropylene connector to the tube. Curing was done in an oven at 120 °C. 18 gauge Teflon tubes with female luer connectors, from Hamilton Company,[10] were attached to the barb-to-male luer connectors for gas and liquid flow. Fig. 6 further elucidates the connector fabrication process.

The strength of the interconnector was characterized by pull-out tests described in Section 4.2.

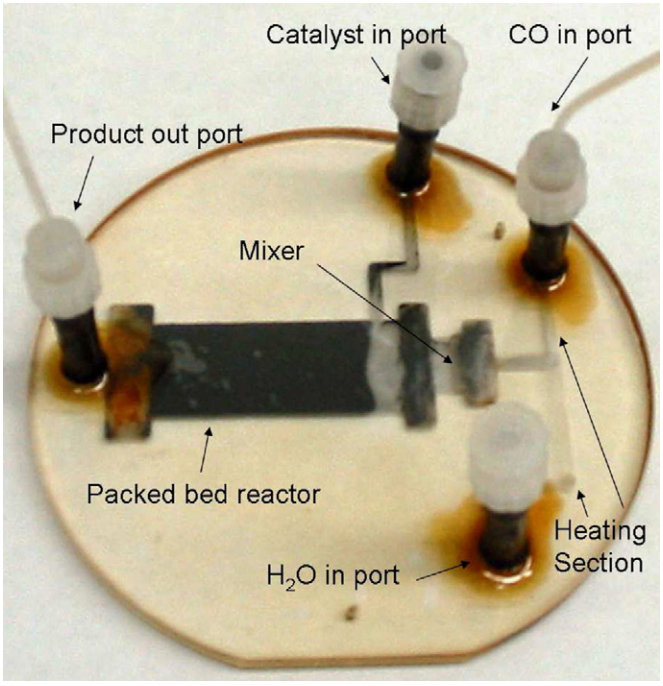

Fig. 5. Photograph of microreactor.

3.4. Flow distribution

A clear understanding of the fabricated device could not be accomplished in its entirety by empirical means alone. The gas phase colorless nature of the reacting fluids prevented any kind of visual characterization of the flow pattern. The flow patterns were therefore simulated.

The reactants flow from the 1 mm broad heater-mixer channel into a broader mixer section and eventually into the reactor section. Flow distribution is facilitated by a glass wool filter. Non-uniform gas flow would lead to sub-optimal mixing and lower reaction conversion. Therefore the issue of uniform gas velocity is critical in the design. Several other flow distribution designs have been proposed in the past (see for example Amador et al. [35], Ajmera et al. [9] and Commenge et al. [36]). The present method proposed is substantially simpler, but as effective with the use of a glass wool which acted as a porous filter as well as flow distributer.

Darcy's Law was used to simulate the porous filter area. Darcy's Law states that,

$$\mathbf{u} = -\frac{K''}{\mu}\nabla P. \tag{8}$$

Here, K'' denotes the permeability of the porous media, μ the fluid viscosity, P the pressure and $\mathbf{u}$ is the velocity vector of the gas mixture. The inlet velocity for the simulation is 1.667 m/s. For a cross-sectional area of 1000 μm × 600 μm, this fluid velocity corresponds to a volumetric flow of 60 ml/min at NTP or 0.146 mol/h of CO-steam mixture. The viscosity used for the simulation is 1.2×10^5 kg/m/s.

The continuity equation for incompressible flow is assumed which is,

$$\nabla \cdot \mathbf{u} = 0. \tag{9}$$

Combining Eqs. (8) and (9), we get,

$$\nabla \cdot \left(-\frac{K''}{\mu}\nabla P \right) = 0. \tag{10}$$

The system was simulated using FEMLAB, a modeling software that uses finite element analysis to numerically integrate coupled partial differential equations. A 2D approximation was assumed. An approximate value of the constant K'' was obtained by comparing simulation pressure drop with experimentally measured values (see Fig. 7). Using this value of K'' the flow velocity in the system was calculated. Clearly, from the FEMLAB generated results in Fig. 8 we see that the outlet velocity is uniform as indicated by the "equal velocity contours".

The method for evaluating permeability was not accurate and at best an approximation. To confirm that uniform flow distribution is indeed achieved, the flow distribution was re-simulated using permeability constant which is double the original K'' value. This simulation again leads to uniform flow distribution indicating that the accuracy of K'' evaluation is not critical to uniformity of flow.

This study clearly demonstrates that the flow field is uniform due to the presence of the glass wool filter. This flow distribution method was exploited in designing a micro-mixer explained in the next section.

[9] http://www.harvardapparatus.com/.
[10] http://www.hamiltoncompany.com/product/syringe/tubing.html.

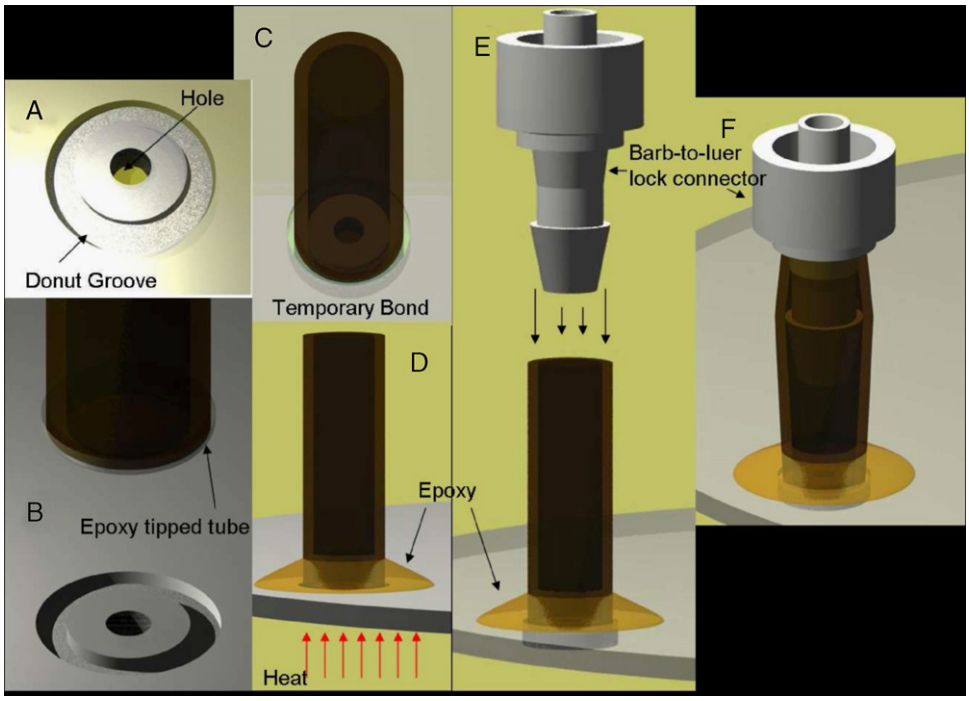

Fig. 6. Steps in macro-micro fluidic connector fabrication. (A) Through hole and doughnut groove is machined in glass. (B and C) Epoxy tipped Teflon tube is placed on the doughnut groove and cured. (D) More epoxy is poured on the outside and then cured. (E and F) Barb-to-luer connector is pushed into the tube.

3.5. Micro-mixer

An effective micro-mixer (see Fig. 1) is proposed to mix CO and steam. This mixer design is based on the limitations of the fabrication method proposed in Section 3.2. In this the width of the channel is constrained by the width of the drill bit. In this work, the minimum drill bit diameter used is 1 mm. The depth of the channel, however, can be much smaller. In this work, the minimum depth of channel is 100 μm.

The design of the micro-mixer, illustrated in Fig. 9, is based on the principal of increasing the surface area of contact of the two fluids. The principal part of the design is the expander section. Here the fluid enters from a smaller channel (in the heating section) and expands into a broader section. An analysis of flow expansion or distribution is given in Section 3.4. The flow from a smaller channel to a larger channel substantially reduces the flow velocity, as illustrated in Fig. 9A and B. The streamlines shown in Fig. 9B are color coded so that yellow indicates highest velocity and dark blue indicates lowest velocity. The flattened/expanded fluid channels come together in the joining section and then mix completely in the mixing section. The larger area of contact significantly enhances the fluid mixing. In Fig. 9C the extent of mixing is indicated by color variation. Yellow indicates steam, black indicates CO and orange indicates completely mixed gases.

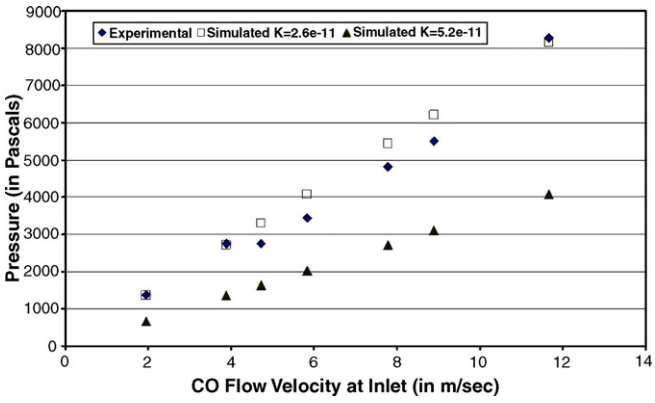

Fig. 7. Pressure drop comparison between simulation and experiment.

The Fourier number can be used for preliminary evaluation of the mixing length. The modified Fourier equation (see for example Ref. [2]) can be stated as,

$$L = \frac{F_o v_g D_c^2}{D_{ab}}. \tag{11}$$

Here, v_g is the velocity of gas flow, L the length of mixing and D_{ab} is the diffusivity constant. For complete mixing, Fourier number, F_o, has to be greater than or equal to 1. The objective is to reduce mixing length, L. In this mixer this objective is achieved by decreasing the flow velocity, v_g, as also the characteristic height, D_c, which is half the thickness of the mixing channel or 50 μm. Assuming total volumetric flow rate of 60 ml/min, and cross-sectional area of 1×10^{-6} m^2 (i.e. 10 mm broad and 0.1 mm thick), we get v_g to be 1 m/s (see Fig. 9A). Assuming the diffusivity co-efficient, D_{ab}, to be 1×10^{-5} and Fourier number, F_o, to be 1, from Eq. (11), we get L to be a 0.25 mm (see Fig. 9B). In this work, the mixing section is 5 mm in length.

For a T-mixer, fabricated using the same method, the characteristic length, D_c, would be half the width of the channel

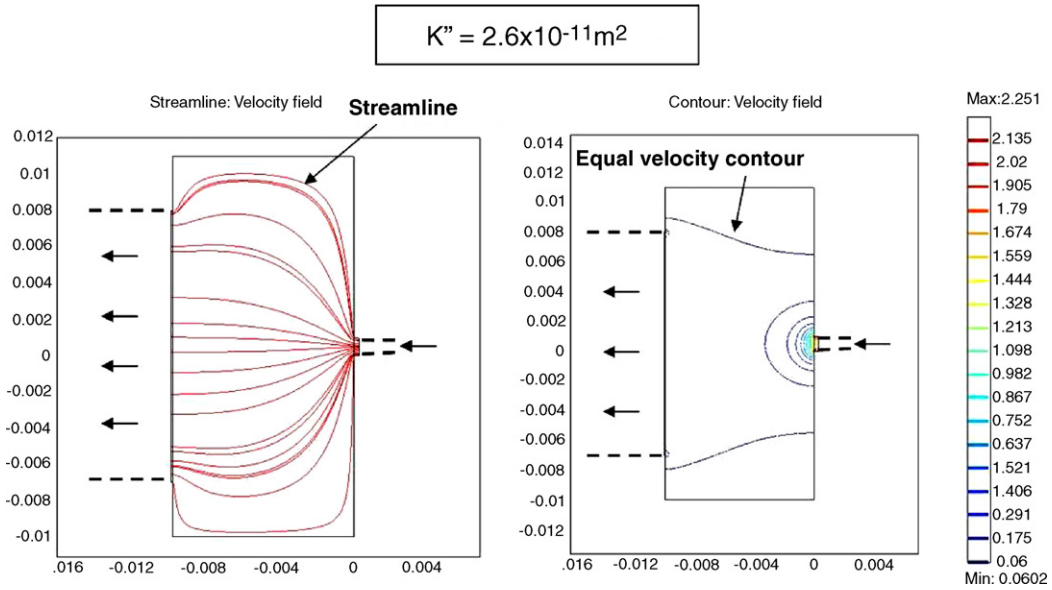

Fig. 8. Flow distribution simulation result with $K'' = 2.6 \times 10^{-11}$ m^2.

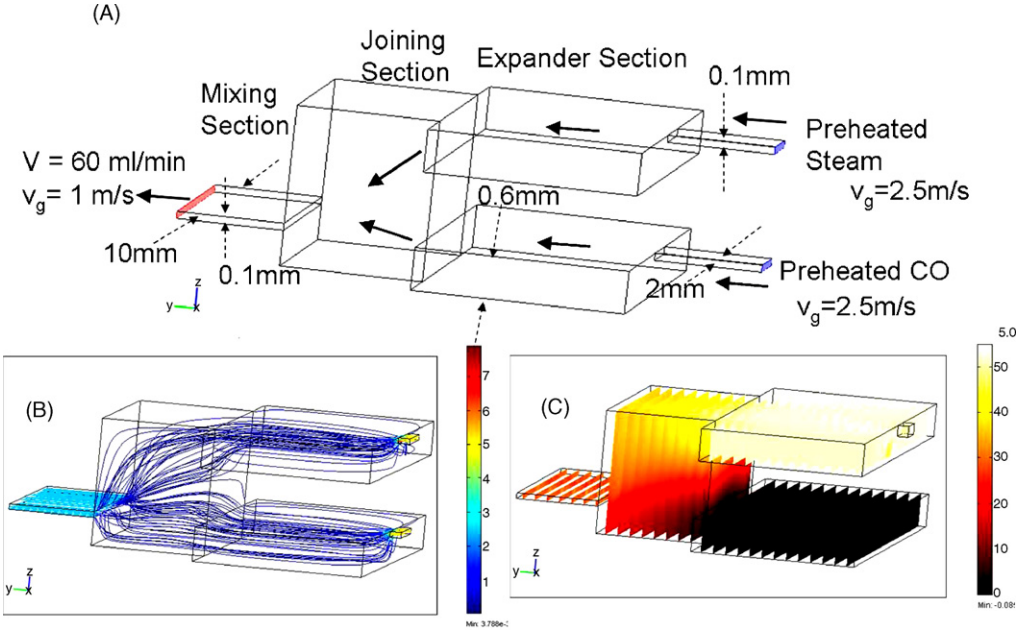

Fig. 9. Micro-mixer. (A) The micro-mixer consists of the expander section, joining section and the mixing section. (B) Approximate flow streamlines. (C) Approximate extent of mixing at various sections of the mixer.

or 0.5 mm. For the same gas volumetric flow rate of 60 ml/min, and cross-sectional area of 5×10^{-7} m^2 (i.e. 1 mm broad and 0.5 mm thick[11]), the gas flow velocity is 2 m/s (see Fig. 10). Assuming the diffusivity co-efficient is same, from Eq. (11) we get the expected mixing length, L, to be 50 mm. This calculation clearly demonstrates that the proposed mixer is significantly better than a T-mixer.

[11] For T-mixers, thicker channels lead to lower velocity and reduced mixing length.

3.6. Evaporation

Vaporization of water is instantaneous at the inlet port and this leads to rapid increase of volume or pressure surges. At 2 atm pressure, the volume increases by a factor of 850. This sudden increase in volume is an unacceptable phenomenon as it damages and weakens the glass structure. More importantly, the sudden change in volume leads to cyclic pressure surges, which is characterized by discontinuous flow of steam into the reactor. This in turn leads to bad mixing and reduced conversion.

Micro-vaporization reported in literature (see Ferret et al. [37]) has followed a distinct approach of attempting to increase surface area. In Ref. [37] surface area for boiling was increased by using 200 μm channels in silicon. The solutions proposed there led to problem like fouling and pressure surges. The conclusion reached was that a porous media type of structure might be optimum.

In our work, a glass wool/Cu metal wire vaporization section was built (see Fig. 1). The use of two materials of distinctly different thermal conductivity (i.e. glass wool and Cu metal) was particularly advantageous. Metal wires were placed at the end of the vaporization section, while glass wool was used close to the water inlet. The large surface area of the glass wool absorbs the water and delays the vaporization, increases the surface area of vaporization and helps prevent pressure surges that could damage the reactor. Furthermore, glass wool was stuffed into the tube of the inlet port to further deaden the pulsation. The metal wire helps increase the surface area of vaporization. The 13 mm × 7 mm × 0.6 mm vaporizer was used to vaporize 0.035 ml/min of water with no visible pulsation.

3.7. Catalyst packing

Finally, commercial WGSR catalyst from Synetix[12] was crushed and sieved to 50–75 μm diameter, and fluidized into the reactor. For this, the catalyst particles were poured into the "catalyst in" port (see Fig. 5). The outlet port and inlet ports were connected to vacuum and the "catalyst in" port was connected to a compressed nitrogen line. The catalyst particles collected in the inlet port got fluidized into the reactor section. Here they were retained by the glass wool filter.

4. Characterization

4.1. Pressure test

Before packing the microreactor with catalyst, the microchannel structure was subjected to pressure tests, to ensure that no leaks existed and also to determine the pressure that the unit could withstand. Two tests were carried out, the gas test and the water test.

In the gas test, the unit was pressurized with argon and submerged in water. No bubbles were observed indicating no leakages. The unit could be pressurized to 345 kPa.

The unit was tested for higher pressure using water. The inlet was connected to a syringe pump and water was pumped into the unit. A pressure sensor was used to measure the ultimate pressure. Once the trapped air was removed, the outlet port was sealed. The unit was slowly pressurized. In the case when the barb connector was not reinforced with epoxy, the barb-to-luer connector came off at 1.48 MPa, clearly indicating the most sensitive section. When the connector was reinforced with epoxy, the pressure went up to 1.65 MPa. This was the limit of the testing apparatus.

[12] http://www.synetix.com/refineries/hydrogen-lowtempshift.htm.

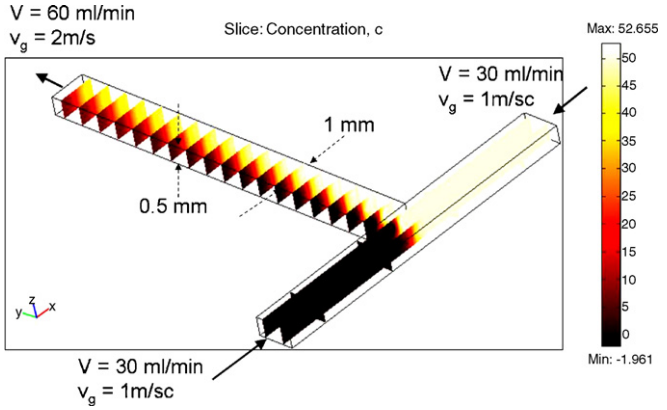

Fig. 10. Comparative T-mixer showing dimensional assumptions. Yellow and black indicate unmixed fluids, while orange/grey is fully mixed.

Due to testing limitations, though the ultimate pressure could not be measured, the unit could safely withstand up to 1.65 MPa, which is much higher than that required for the Water Gas Shift Reaction experiments that this unit was used for. Further, these tests validated the use of epoxy as a bonding agent for the two wafers and the microfluidic connector proposed above.

4.2. Pull-out test

The strength of the microfluidic connector described above was tested by the pull-out test. The pull-out test, as the name suggests, determines the ultimate force with which the connector can be pulled before breaking. The strength of the bond can thus be tested. Force was applied in two orthogonal directions: perpendicular to the plane of the wafer and parallel to the plane of the wafer. An 18 guage Teflon capillary with female luer lock at one end was used to connect the connector to the counterbalancing force.

Vertical force was applied to the connector using counterweight. The weight was slowly increased in increments of 200 g, until the total weight was 2.625 kg or a force of 25.73 N was applied. At this force the 18 gauge Teflon tube tore but the connector remained intact. The testing set-up thus limited the evaluation of the ultimate force the connector could withstand.

A similar test was carried out with a force in the orthogonal direction. The force applied created a torque about the base of the connector. The ultimate weight applied was 1.226 kg or 12.013 N force. At that force the Teflon tube bent but no leaks were perceived.

These tests clearly demonstrated that the Teflon bond to the wafer was sufficiently robust for our use and usual amount of pull or tug would not affect it. The experiments described above closely resemble short-term static loading described in Young and Budynas [38].

4.3. Pressure drop characterization

The packed bed of catalyst leads to significant pressure drop in the gas flow. For accurate characterization of the reaction rate, pressure drop in the reactor needs to be characterized and correlated.

The set-up for the pressure drop characterization consists of pressure transducers at the inlet and outlet of the unit. The difference in the readings gives the pressure drop. Carbon monoxide from a cylinder was passed through a mass flow controller, via a pressure sensor into the unit. The pressure drop was first measured for the case where there was no catalyst in the system. The pressure drop was found to be negligible. Then the catalyst was filled as described above. The pressure drop characterization was done at room temperature and at various temperatures between 160 and 220 °C, which is close to reaction conditions.

The results of the tests were correlated with the Ergun equation. For low *Re* numbers, the Ergun equation (see Scott Fogler [39]) for an unidirectional flow can be approximated to be:

$$\frac{dP}{dl} = -\frac{150V\mu}{D_p^2 A_c}\frac{(1-\phi)^2}{\phi^3}. \tag{12}$$

The variation of velocity (V) along the length of the channel (l) needs to be considered for accurate derivation of the pressure drop (dP/dl) equation. In the above equation D_p, μ and ϕ represent particle diameter, viscosity and porosity. Assuming ideal gas law is valid, applying it to Eq. (12) and then integrating we get:

$$\frac{P_i^2 - P_o^2}{2LP_0} = \frac{150V_0\mu}{D_p^2 A_c}\frac{(1-\phi)^2}{\phi^3}\frac{T}{T_0}. \tag{13}$$

Here P_o and P_i refer to the pressure reading in the inlet and outlet and the subscript 0 refers to normal temperature and pressure (NTP) values. Eq. (13) can now be restated as:

$$\frac{P_i^2 - P_o^2}{P_0^2} = K'LV_0. \tag{14}$$

The above equation has been plotted in Fig. 11. Clearly the experimental data corroborates the validity of Eq. (14). The quantitative value of correlation function K' was not explicitly used in our study. Rather, Eq. (14) has been used in the Appendix A to derive the reaction rate constant (Eq. (6)).

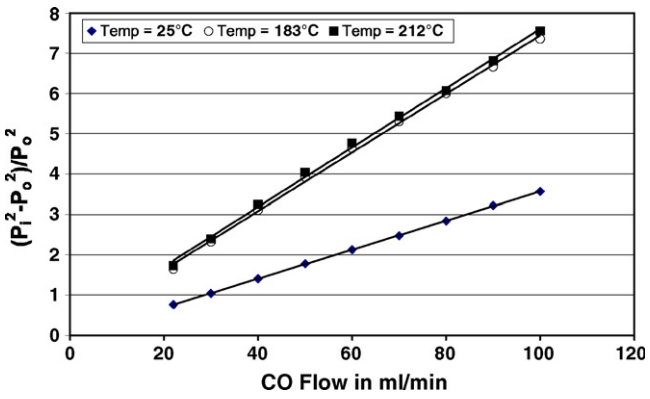

Fig. 11. Pressure drop correlation. See Eq. (14).

Table 2
Experimental conditions

Reactor parameters	Values (units)
Water flow rate	0.014–0.027 ml/min
CO volumetric flow rate	18–29 ml/min (NTP)
Temperature	185–250 °C
Catalyst weight	0.49 g
Particle diameter	50–75 μm

5. Catalyst activation and reaction results

Details of the experimental set-up have been given earlier in Section 3.1. The experimental conditions are given in Table 2.

5.1. Catalyst activation

The catalyst was fluidized into the reactor and activated by flowing 20% hydrogen, 80% nitrogen into the reactor and heating it. The heating was done in two stages. Initially the reactor was heated at 175 °C for 4 h and then at 220 °C for 16 h.

5.2. Results

Water Gas Shift Reaction was carried out under a variety of conditions. The operating variables that were modified were temperature (T), the water to carbon monoxide flow ratio (M), and the total flow rate with constant reactant composition. Additionally an experiment was carried out wherein the total flow rate was kept constant, but the molar ratio of the reactants (M) was varied. The operating conditions are given in Table 2. The results of the experiment can be seen in Figs. 12–15.

In Fig. 12, the flow rate of carbon monoxide was kept constant at 24 ml/min (NTP) or 0.6 mol/h while the molar water ratio (M) was varied between 0.78 and 1.23. The experiment was varied for three different temperatures. Intuitively, when the reactant, water, is increased, the hydrogen production also increases. Conversely, with increase in water flow, the space–time decreases. The overall effect was that of increase of reaction conversion with increase of water flow.

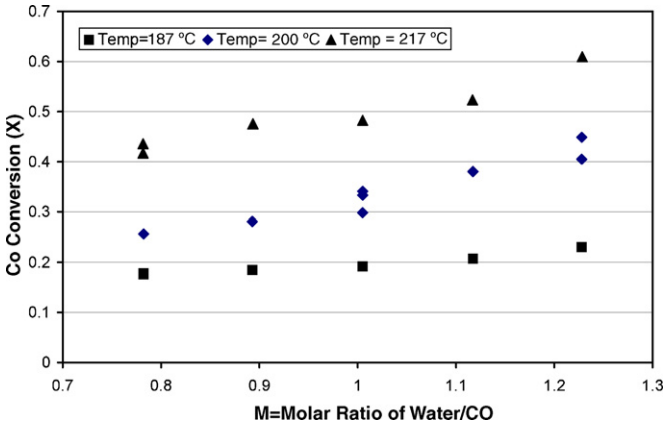

Fig. 12. Reaction conversion with constant CO flow and varying reactant ratio (M).

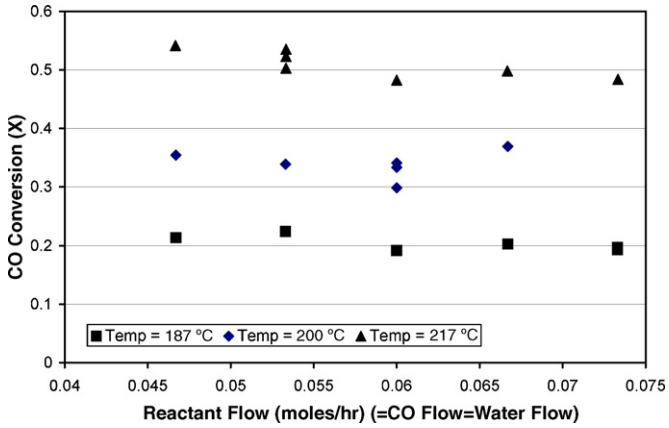

Fig. 13. Reaction conversion with equimolar reactant flow.

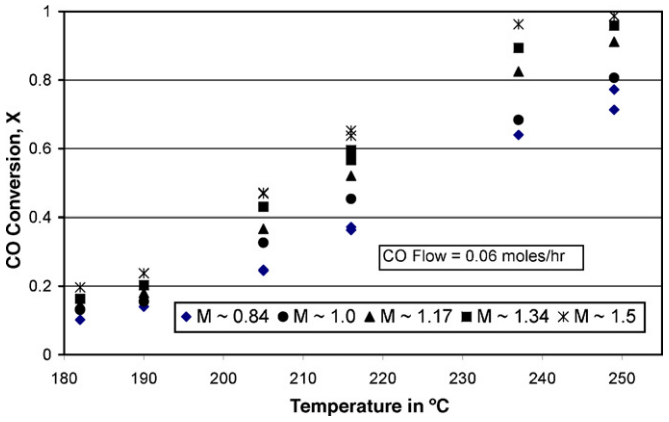

Fig. 15. Conversion with varying temperature.

In Fig. 13, the molar flow rate ratio of CO and water was kept constant and the total flow was varied. The space–time was therefore changed. The graph confirms that reduced space–time leads to reduced conversion. In Fig. 15 the total flow rate was kept constant while the carbon monoxide and water ratio was varied.

Finally the effect of temperature variation was explored in Fig. 14. Reaction was carried out at five different molar ratios ranging from 0.84 to 1.5. It was found that at 240 °C, the conversion came close to equilibrium for CO flow rate of 0.6 mol/h and water-to-CO ratio (M) of 1.5.

Each data point that was presented in Fig. 12 was based on a reading that was constant over 20 min. The reaction was sometimes affected by disturbances. This leads to slight variation in conversion over time. These results have been reported with multiple ordinates for the same abscissa.

Inaccuracy in measurement led to certain amount of error which was carefully analyzed. The greatest source of error is the drift in the mass spectrometer over time. To reduce error all experiments were carried out over a 2-week period and the error was found to be within acceptable bounds of accuracy.

5.3. Reaction analysis

The data obtained from reaction run were plotted in Figs. 12–15, and subsequently used to find the rate constant, K.

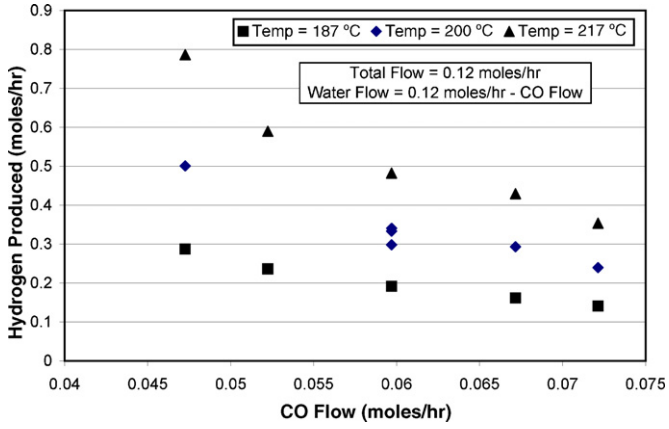

Fig. 14. Total flow was kept constant, while ratio of the reactants was varied.

For this the data was fitted to two separate rate expressions. The rate constants obtained from the fitting are shown in Eqs. (15) and (19).

5.3.1. Reversible rate expression

A reversible rate expression was modified to explicitly incorporate the pressure variation along the length of the reactor (see Appendix A). This rate expression is given in Eq. (6). The data from the reaction runs were fitted to the rate expression and plotted in Fig. 16. From the plot, an approximate Arrhenius type rate constant was obtained which can be stated as,

$$\ln(K) = -\frac{E}{RT} + \ln(A) = -\frac{11425}{T} + 20.7079. \quad (15)$$

Here A has the units of l^2/(g mol s) and E/R has the units of temperature, in Kelvin. It was found that variation in steam flow lead to greater deviation from the fitted line than CO flow. The value of E/R is significantly different from that reported in literature. Mann et al. [40] and Keiski et al. [30] who have used similar catalyst, for example, report values of −5755 and −5557 K.

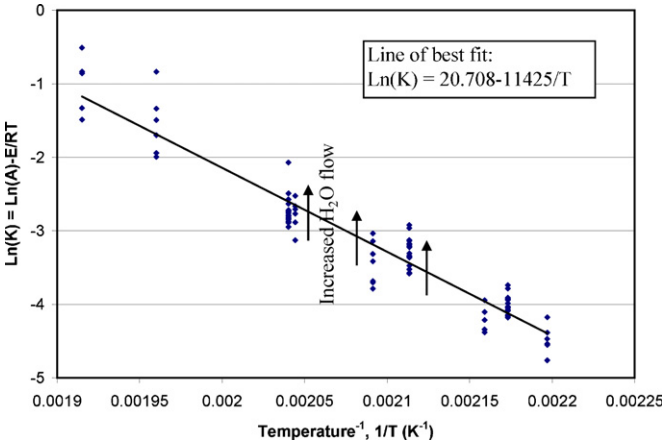

Fig. 16. Reaction conversion results are used to evaluate the reaction rate by using Eq. (4). Variation in water flow seemed to cause greater deviation from the line-of-best-fit.

Table 3
Comparison of reaction rate with literature [40]

	Results from Mann et al. [40]	Results from this work
Arrhenius correlation	$\ln(K) = 1.487 - 5755/T$	$\ln(K) = 14.163 - 12005/T$
K (at 200 °C)	2.3095×10^{-5}	1.3548×10^{-5}
K (at 210 °C)	2.9706×10^{-5}	2.2905×10^{-5}
K (at 220 °C)	3.7821×10^{-5}	3.7909×10^{-5}

5.3.2. Rate expression proposed by Mann et al. [40]

The reaction conversion results were verified by fitting them to the rate equation proposed by Mann et al. [40]:

$$r_{CO} = \frac{K_{exp}(p_{CO}\, p_{H_2O}/p_{H_2}^{1/2})(1 - p_{H_2}\, p_{CO_2}/(K_{eq}\, p_{CO}\, p_{H_2O}))}{(1 + K_1\, p_{CO_2}\, p_{H_2}^{1/2} + K_2\, p_{H_2O}/p_{H_2}^{1/2})^2}. \tag{16}$$

Here p_{CO}, p_{H_2O}, p_{H_2} and p_{CO_2} are the partial pressures of carbon monoxide, steam, hydrogen and carbon dioxide respectively and K_{exp} is a modified rate constant that is defined by Eq. (18). Here K_1 and K_2 are thermodynamic parameters which have been stated as (see Ref. [40]):

$$K_1 = \exp\left[9.12 - \frac{4870}{T}\right]; \qquad K_2 = \exp\left[-3.28 + \frac{854}{T}\right]. \tag{17}$$

Active copper surface area was assumed to be (see Ref. [40]) 7.3×10^3 m^2/kg and further a correction for CO concentration was made, where K_{exp} in Eq. (16) was replaced by,

$$K = K_{exp}\left[1 + \frac{636\, p_{CO\text{-}av}}{T}\right]^2. \tag{18}$$

Here $p_{CO\text{-}av}$ is the average CO partial pressure in the reactor and assumed to be half the inlet and outlet partial pressures. The rate constant obtained by fitting can be expressed as:

$$\ln(K) = -\frac{E}{RT} + \ln(A) = -\frac{12005}{T} + 14.163. \tag{19}$$

Here the rate constant, K, has the units of mol s^{-1} (m^2 of active Cu)$^{-1}$ bar$^{-3/2}$. The result of fitting is analyzed in Table 3. Clearly there is deviation in the pre-exponential constant, A, and the activation energy, E. However, the rate constants, K, have similar values at the range of reaction temperature. This clearly validates the experimental results.

6. Conclusion

A compact glass based microreactor for Water Gas Shift Reaction was successfully developed. As part of the microreactor, a novel macro-micro fluidic connector was demonstrated. The unit was thoroughly characterized for strength, pressure drop and reaction conversion. It was found that the glass microreactor was adequately strong, the pressure drop followed the Ergun equation and reaction rate could be characterized for future design requirements. Moreover, the unit was found to be simple in design, easy to fabricate, fully functional and yet economical. Similar microreactors fabricated with silicon in microfabrication (clean room) facilities could cost as much as US$ 1500[13] for each reactor. In comparison, the proposed glass reactor needed less than US$ 100[14] to fabricate making it ideal for first generation prototyping work. Successful fabrication in the first attempt underlines the ease in fabrication. Though 50–75 μm particle sized catalyst was used in this study, significantly smaller catalyst size could also be used. Finally the reactor was extensively characterized under a range of conditions and the rate constant derived was found to match closely to values found in literature. The proposed fabrication process could be potentially applied to other catalyst testing micro chemical systems.

Further improvements can be made to the unit. The hot plate presently used to heat the reactor can be replaced by metal heating lines. Thermal sensors can also be incorporated. Moreover, the system can be insulated for better energy balance. Epoxy presently used for bonding the glass can be replaced by diffusion bonding for applications that need to operate at higher temperature. The barbed connector used in this study can be replaced by Swagelock connectors, which could improve the temperature and pressure limit.

Acknowledgements

The authors would like to acknowledge the assistance provided by Joe Zelinski (Lehigh University's Physics Department Machine Shop) in drilling the glass wafers and Synetix for providing the Katalco 83—3K WGSR catalyst. This work was supported by funding from National Science Foundation (XYZ-on-a-chip initiative grant CTS-9980781), Pittsburgh Digital Greenhouse and Sigma-Xi Grant-in-Aid of Research.

Appendix A. Derivation of Eq. (6)

The reaction rate assumed for this plug flow reactor has been stated in Eq. (4). The assumed geometry has been further explained in Fig. 17. Assuming ideal gas law, the concentration of CO at point l along the length of the reactor can be stated as:

$$C_{CO} = \frac{P n_{CO}(1 - X)}{RT(n_{CO} + n_{H_2O} + n_{H_2} + n_{CO_2})}. \tag{A.1}$$

For an equimolar reaction, this can be restated as:

$$C_{CO} = \frac{P n_{CO}^0(1 - X)}{RT(n_{CO}^0 + n_{H_2O}^0)} = \frac{P(1 - X)}{RT(1 + M)}. \tag{A.2}$$

[13] US$ 1500 cost of fabrication assumes 20 h needed to fabricate at US$ 75 per hour for fabrication.
[14] US$ 100 cost of the proposed reactor is based on US$ 13 per hour for 3 h in a machine shop.

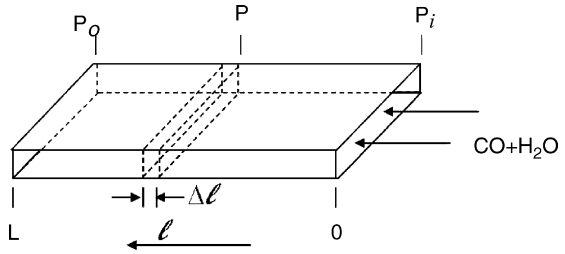

Fig. 17. Schematic diagram of rectangular reactor.

Similarly, the other reactant concentrations at point l in the reactor can be expressed as:

$$C_{H_2O} = \frac{Pn^0_{CO}(M - X)}{RT(n^0_{CO} + n^0_{H_2O})} = \frac{P(M - X)}{RT(1 + M)}, \quad (A.3)$$

and

$$C_{H_2} = C_{CO_2} = \frac{Pn^0_{CO}X}{RT(n^0_{CO} + n^0_{H_2O})} = \frac{PX}{RT(1 + M)}. \quad (A.4)$$

Inserting Eqs. (A.2)–(A.4) in Eq. (4), we get,

$$n^0_{CO}\frac{dX}{dl} = \frac{WK}{L}\left(\frac{P(1 - X)}{RT(1 + M)}\frac{P(M - X)}{RT(1 + M)} - \left(\frac{PX}{RT(1 + M)}\right)^2 \frac{1}{K_{eq}}\right). \quad (A.5)$$

Assuming isothermality, the variables can be reassembled and restated as:

$$\frac{1}{1 - (1/K_{eq})}\int_0^{X_L} \frac{dX}{(X - X_1)(X - X_2)} = \frac{WK}{Ln^0_{CO}(RT)^2(1 + M)^2}\int_0^L P^2\, dl. \quad (A.6)$$

Here X_1 and X_2 are defined as solutions to Eq. (7). The pressure correlation has been given by Eq. (14). For pressure, P, at any point l, this can be restated as:

$$\frac{P_i^2 - P^2}{P_0^2} = KlV_0. \quad (A.7)$$

Combining Eqs. (14) and (A.7), we get

$$P^2 = \frac{L - l}{L}(P_i^2 - P_o^2) + P_o^2. \quad (A.8)$$

Inserting Eq. (A.8) in Eq. (A.6), and then integrating we get,

$$\frac{1}{\sqrt{(1 - M)^2 + (4M/K_{eq})}}\ln\left(\frac{(X_L - X_2)X_1}{(X_L - X_1)X_2}\right) = \frac{WK}{n^0_{CO}(RT)^2(1 + M)^2}\left(\frac{P_i^2 + P_o^2}{2}\right). \quad (A.9)$$

Eq. (6) follows. Eq. (A.9) is similar to the equation derived by Moe [29].

References

[1] E.R. Delsman, M.H.J.M. de Croon, G.J. Kramer, P.D. Cobden, Ch. Hofmann, V. Cominos, J.C. Schouten, Experiments and modeling of an integrated preferential oxidation-heat exchanger microdevice, Chem. Eng. J. 101 (August (1–3)) (2004) 123–131.

[2] D. Gobby, P. Angeli, A. Gavriilidis, Mixing characteristics of T-type microfluidic mixers, J. Micromech. Microeng. 11 (March (2)) (2001) 126–132.

[3] S. Hardt, F. Schönfeld, Laminar mixing in different interdigital micromixers. II. Numerical simulations, AIChE 49 (March (3)) (2003) 578–584.

[4] M.W. Losey, R.J. Jackman, S.L. Firebaugh, M.A. Schmidt, K.F. Jensen, Design and fabrication of microfluidic devices for multiphase mixing and reaction, J. Microelectromech. Syst. 11 (December (6)) (2002) 709–717.

[5] P.D.I. Fletcher, S.J. Haswell, E. Pombo-Villar, B.H. Warrington, P. Watts, S.Y.F. Wong, X. Zhang, Micro reactors: principles and applications in organic synthesis, Tetrahedron 58 (June (24)) (2002) 4735–4757.

[6] S. Schirrmeister, G. Markowz, DEMIS: demonstrating the technical feasibility of heterogeneous gas phase catalysis in micro structured reactors on the pilot scale, in: Seventh International Conference on Microreaction Technology (IMRET 7), Lausanne, Switzerland, September, (2003), pp. 49–50.

[7] M. Matlosz, Integrated multiscale process units with locally structured elements, in: IMRET 8: Proceedings of the Eighth International Conference on Microreaction Technology, Atlanta, GA, April, 2005.

[8] A.L. Tonkovich, S. Fitzgerald, R. Arora, Commercial scale microchannel technology methodology and capabilities, in: IMRET 8: Proceedings of the Eighth International Conference on Microreaction Technology, Atlanta, GA, April, 2004.

[9] S.K. Ajmera, C. Delattre, M.A. Schmidt, K.F. Jensen, Microfabricated differential reactor for heterogeneous gas phase catalyst testing, J. Catal. 209 (July (2)) (2002) 401–412.

[10] K. Shah, W.C. Shin, R.S. Besser, Novel microfabrication approaches for directly patterning PEM fuel cell membranes, J. Power Sources 123 (September) (2003) 172–181.

[11] A. Heinzel, C. Hebling, M. Muller, M. Zedda, C. Muller, Fuel cells for low power applications, J. Power Sources 105 (March (2)) (2002) 250–255.

[12] A.V. Pattekar, M.V. Kothare, A microreactor for hydrogen production in micro-fuel cell applications, J. Microelectromech. Syst. 13 (February (1)) (2004) 7–18.

[13] J.D. Holladay, E.O. Jones, M. Phelps, J. Hu, Microfuel processor for use in a miniature power supply, J. Power Sources 108 (June (1–2)) (2002) 21–27.

[14] S. Fitzgerald, R. Wegeng, A. Tonkovich, Y. Wang, H. Freeman, J. Marco, G. Roberts, D. VanderWeil, A compact steam reforming reactor for use in an automotive fuel processor, in: I. Rinard, W. Ehrfeld, U. Eul, R.S. Wegeng (Eds.), Proceedings of the Fourth International Conference on Microreaction Technology, Atlanta, GA, March 5–9, (2000), pp. 358–363.

[15] A. Mitsos, I. Palou-Rivera, P.I. Barton, Alternative for micropower generation processes, Ind. Eng. Chem. Res. 43 (January (1)) (2004) 74–84.

[16] S.V. Karnik, M.K. Hatalis, M.V. Kothare, Towards a palladium micromembrane for the water gas shift reaction: microfabrication approach and hydrogen purification results, J. Microelectromech. Syst. 12 (February (1)) (2003) 93–100.

[17] R. Hakkarainen, T. Salmi, R.L. Keiski, Comparison of the dynamics of the high-temperature water-gas shift reaction on oxide catalysts, Catal. Today 20 (August (3)) (1994) 395–408.

[18] N.E. Amadeo, M.A. Laborde, Hydrogen production from the low-temperature water-gas shift reaction: kinetics and simulation of the industrial reactor, Int. J. Hydrogen Energy 20 (December (12)) (1995) 949–956.

[19] M.J.L. Gines, A.J. Marchi, C.R. Apesteguia, Kinetic study of the reverse water-gas shift reaction over $CuO/ZnO/Al_2O_3$ catalysts, Appl. Catal. A: Gen. 154 (1997) 155–171.

[20] D.E. Mears, Tests for transport limitation in experimental catalytic reactors, Ind. Eng. Chem. Process Des. Devel. 10 (4) (1971) 541–547.

[21] D.E. Mears, Diagnostic criteria for heat transport limitation in fixed bed reactors, J. Catal. 20 (1971) 127–131.

[22] Y. Choi, Optimized fuel cell grade hydrogen from methanol, Ph.D. Thesis, Department of Chemical Engineering, Lehigh University, Bethlehem, November 2003.
[23] O. Goerke, P. Pfeifer, K. Schubert, Water gas shift reaction and selective oxidation of CO in microreactors, Appl. Catal. A: Gen. 263 (May (1)) (2004) 11–18.
[24] J. Bravo, A. Karim, T. Conant, G.P. Lopez, A. Datye, Wall coating of a $CuO/ZnO/Al_2O_3$ methanol stream reforming catalyst for micro-channel reformers, Chem. Eng. J. 101 (August) (2004) 113–121.
[25] M. Brivio, R.E. Oosterbroek, W. Verboom, M.H. Goedbloed, A. van der Berg, D.N. Reinhoudt, Surface effects in the esterification of 9-pyrene-butyric acid within a glass micro reactor, Chem. Commun. (July (15)) (2003) 1924–1925.
[26] X. Li, T. Abe, Y. Liu, M. Esashi, Fabrication of high-density electrical feed-throughs by deep-reactive-ion etching of pyrex glass, J. Microelectromech. Syst. 11 (December (6)) (2002) 625–630.
[27] T.R. Dietrich, W. Ehrfeld, M. Lacher, M. Krämer, B. Speit, Fabrication technologies for microsystems utilizing photoetchable glass, Microelectron. Eng. 30 (1996) 497–504.
[28] Y.-R. Cho, J.-Y. Oh, H.-S. Kim, H.-S. Jeong, Micro-etching technology of high aspect ratio frameworks for electronic devices, Mater. Sci. Eng. B 64 (September (2)) (1999) 79–83.
[29] J.M. Moe, Design of water-gas shift reactors, Chem. Eng. Prog. 58 (March (3)) (1962) 33–37.
[30] R.L. Keiski, O. Desponds, Y.F. Chang, G.A. Somorjai, Kinetics of the water-gas shift reaction over several alkane activation and water-gas shift catalysts, Appl. Catal. A: Gen. 101 (1993) 317–338.
[31] A. Karim, J. Bravo, A. Datye, Nonisothermality in packed bed reactors for steam reforming of methanol, Appl. Catal. A: Gen. 282 (2005) 101–109.
[32] H. Tsai Jr., L. Lin, Micro-to-macro fluidic interconnectors with an integrated polymer sealant, J. Micromech. Microeng. 11 (2001) 577–581.
[33] H. Andersson, W. van der Wijngaart, P. Enoksson, G. Stemme, Micromachined flow-through filter chamber for chemical reactions on beads, Sens. Actuators B: Chem. 67 (2000) 203–208.
[34] A.V. Pattekar, M.V. Kothare, Novel microfluidic interconnectors for high temperature and pressure applications, J. Micromech. Microeng. 13 (January) (2003) 337–345.
[35] C. Amador, A. Gavriilidis, P. Angeli, Flow distribution in different microreactor scale-out geometries and the effect of manufacturing tolerances and channel blockage, Chem. Eng. J. 101 (2004) 379–390.
[36] J.M. Commenge, L. Falk, J.P. Corriou, M. Maltosz, Optimal design for flow uniformity in microchannel reactors, AIChE J. 48 (2) (2002) 345–356.
[37] C. Ferret, L. Falk, U.D. Ortona, A. Chenu, T.T. Veenstra, Introduction of image analysis for the quantification of the boiling flow heat transfer, Chem. Eng. J. 101 (2004) 357–365.
[38] W. Young, R. Budynas, Roark's Formulas for Stress and Strain, McGraw-Hill, New York, NY, USA, 2002.
[39] H. Scott Fogler, Elements of Chemical Reaction Engineering, third ed., Prentice Hall, Upper Saddle River, NJ, 1999.
[40] R.F. Mann, J.C. Amphlett, B. Peppley, C.P. Thurgood, A mechanistic model for the water gas shift reaction over commercial catalysts containing CuO/ZnO, Int. J. Chem. Reactor Eng. 2 (A5) (2004) http://www.bepress.com/ijcre/vol2/A5.